JGR Oceans

RESEARCH ARTICLE

10.1029/2023JC020697

Sea Ice-Driven Iceberg Drift in Baffin Bay

J. M. Marson[1], P. G. Myers[2], A. Garbo[3,4], L. Copland[3], and D. Mueller[4]

[1]University of Manitoba, Winnipeg, MB, Canada, [2]University of Alberta, Edmonton, AB, Canada, [3]University of Ottawa, Ottawa, ON, Canada, [4]Carleton University, Ottawa, ON, Canada

Key Points:

- A new sea ice-iceberg locking parameterization was implemented in Nucleus for European Modeling of the Ocean and tested in a 1/4° resolution regional configuration
- Icebergs locked in sea ice in Baffin Bay are more likely to travel outside of the Baffin Island Current than "unlocked" ones
- The existence of a sea ice locking mechanism in Baffin Bay is supported by observations of co-varying iceberg and sea ice speeds

Supporting Information:

Supporting Information may be found in the online version of this article.

Correspondence to:

J. M. Marson,
Juliana.MariniMarson@umanitoba.ca

Citation:

Marson, J. M., Myers, P. G., Garbo, A., Copland, L., & Mueller, D. (2024). Sea ice-driven iceberg drift in Baffin Bay. *Journal of Geophysical Research: Oceans*, *129*, e2023JC020697. https://doi.org/10.1029/2023JC020697

Received 13 NOV 2023
Accepted 18 APR 2024

Author Contributions:

Conceptualization: J. M. Marson
Data curation: J. M. Marson, A. Garbo, L. Copland, D. Mueller
Formal analysis: J. M. Marson
Funding acquisition: J. M. Marson, P. G. Myers, A. Garbo, L. Copland, D. Mueller
Investigation: J. M. Marson, P. G. Myers
Methodology: J. M. Marson
Project administration: J. M. Marson
Resources: J. M. Marson, P. G. Myers, A. Garbo, L. Copland, D. Mueller
Software: J. M. Marson, P. G. Myers
Supervision: P. G. Myers
Validation: J. M. Marson
Visualization: J. M. Marson
Writing – original draft: J. M. Marson

Abstract Baffin Bay is the travel destination of most icebergs calving from west Greenland. They commonly follow the bay's cyclonic circulation and might end up far south along the coast of Newfoundland and Labrador, where many shipping routes converge. Given the hazard that icebergs pose to marine transportation, understanding their distribution is fundamental. One of the forces driving iceberg drift arises from the presence of sea ice. Observations in the Southern Ocean indicate that icebergs get locked in thick and concentrated sea ice. We present observations that support the occurrence of this sea ice locking mechanism (SIL) in Baffin Bay as well. Most iceberg models, however, represent the sea ice force over an iceberg as a simple drag force. Here, we implement a new parameterization in the iceberg module of the Nucleus for European Modeling of the Ocean (NEMO-ICB) to represent SIL. We show that, by using this new parameterization, icebergs are more likely to travel outside of the Baffin Island Current during winter, which is supported by satellite observations. There is a slight improvement in the representation of iceberg severity along the coast of Newfoundland and Labrador and a slight shift of iceberg melt toward this region and Lancaster Sound/Hudson Strait. Although the impacts of icebergs on sea ice are still not represented, and targeted observations are needed for model calibration regarding sea ice concentration thresholds from which icebergs get locked, we are confident that this model improvement takes iceberg modeling one step forward toward reality.

Plain Language Summary After they break off Greenland's glaciers, icebergs drift in the ocean in somewhat predictable patterns across Baffin Bay. What makes them predictable is that we know the main natural forces that cause icebergs to move: the winds, the ocean currents, and the sea ice cover. Because it is impossible to monitor all the icebergs coming from Greenland, we use computer models to understand their typical trajectories. In these models, each one of the forces responsible for iceberg drift can be represented mathematically, usually in a very simplistic way. The sea ice force, for example, is proportional to how much friction there is between the iceberg and sea ice. However, observations in nature show that the iceberg-sea ice interaction is more complicated than that: if the sea ice cover is thick and compact, it is able to trap icebergs, and both will move as one solid block. In this study, we improve a model's representation of the sea ice force by including this trapping mechanism. Results show that iceberg trajectory can be slightly different during winter due to sea ice trapping and that this mechanism potentially improves our ability to predict when icebergs reach the transatlantic shipping routes east of Canada.

1. Introduction

Made famous after the tragic sinking of RMS Titanic in 1912, icebergs are broadly acknowledged as hazards to navigation and other offshore activities in the North Atlantic (e.g., Bigg et al., 2018; Ding et al., 2021; Hill, 2006). Those icebergs, largely calved from Greenland (Kochtitzky et al., 2022), usually travel through Baffin Bay before reaching the busy shipping lanes over the Grand Banks (offshore eastern Canada, Figure 1). As they calve and melt through their journey, icebergs also impact freshwater distribution in the subpolar North Atlantic (e.g., Martin & Adcroft, 2010), which may alter local-to-regional ocean dynamics (Marson et al., 2021; Yankovsky & Yashayaev, 2014) and marine productivity (Bigg et al., 2021; Hopwood et al., 2019). All of these roles justify a more thorough investigation of their behavior. If we know *where* icebergs go, *when* they arrive there, and *how much* of their mass was lost on the way, we can quantify the icebergs' impacts on marine shipping and on the climate system with more accuracy. Although some North Atlantic icebergs are closely monitored — especially the ones that survive to reach the Grand Banks — observations of iceberg drift and decay upstream in Baffin Bay are not yet comprehensive. Therefore, to understand the general distribution in space and time of Greenland icebergs, we turn to numerical models.

Writing – review & editing:
J. M. Marson, P. G. Myers, A. Garbo, L. Copland, D. Mueller

Since the 1980's, deterministic models have attempted to reproduce icebergs' drift and decay with dynamic and thermodynamic equations that represent their interactions with ocean, atmosphere, and sea ice (e.g., Bigg et al., 1996, 1997; El-Tahan et al., 1988; Løset, 1993; Mountain, 1980; S. D. Smith, 1993; S. D. Smith & Banke, 1983). For iceberg drift, the general form of the dynamic equation in models is:

$$M\frac{d\vec{u}}{dt} = \vec{F}_c + \vec{F}_p + \vec{F}_r + \vec{F}_a + \vec{F}_o + \vec{F}_{si} \quad (1)$$

where the iceberg mass M times its acceleration $d\vec{u}/dt$ is equal to the sum of forces acting on the iceberg, namely: the Coriolis force $\left(\vec{F}_c\right)$, the pressure gradient force $\left(\vec{F}_p\right)$ generated by the sea surface slope, the wave radiation force $\left(\vec{F}_r\right)$, drag forces from the atmosphere $\left(\vec{F}_a\right)$ and the ocean $\left(\vec{F}_o\right)$, and the sea ice force $\left(\vec{F}_{si}\right)$. Although the ocean forcing is recognized as the first-order driver of iceberg drift in most situations (Bigg et al., 1997; Lichey & Hellmer, 2001; Zeinali Torbati et al., 2020), the sea ice forcing might overcome it when icebergs find themselves embedded in pack ice (Hunke & Comeau, 2011; Lichey & Hellmer, 2001; Marko et al., 1994; Morison & Goldberg, 2012; Peterson et al., 2009; Schodlok et al., 2006; Vinje, 1980; Wesche & Dierking, 2016; Yulmetov et al., 2016; Zeinali Torbati et al., 2020).

Vinje (1980) observed how a few Antarctic icebergs tracked through remote sensing moved in synchrony with the highly concentrated sea ice pack, drifting together as a solid block. Similarly, Schodlok et al. (2006) analyzed the drift of icebergs and nearby sea ice floes in the Weddell Sea, and noted that their trajectories are synchronous at sea ice concentrations as low as 86%. Morison and Goldberg (2012) observed the interaction between a small iceberg and sea ice in the Weddell Sea, and also concluded that the iceberg drift was mainly driven by sea ice, with both moving at the same speed. In the Northern Hemisphere, Zeinali Torbati et al. (2020) observed four ice island fragments in the Strait of Belle Isle, eastern Canada. The authors showed that, when sea ice was present at concentrations higher than 20%, it dictated most of the fragments' drift. Moreover, Marko et al. (1994, 2014) associated sea ice cover in Baffin Bay to the seasonal and interannual variability in the number of icebergs reaching the Grand Banks. Keghouche et al. (2010) also observed a correlation between sea ice extent and iceberg presence in the Barents Sea, and Yulmetov et al. (2016) mentioned icebergs being "captured" by landfast ice in northeast Greenland.

While some modeling studies ignore sea ice forcing of icebergs (e.g., Andersson et al., 2016; England et al., 2020; Kubat et al., 2005; Parayil et al., 2022; S. D. Smith, 1993; Turnbull et al., 2015; Wagner et al., 2017), especially if they are focusing on generally ice-free areas, most models (e.g., Bigg et al., 1997; Gladstone et al., 2001; Huth, Adcroft, Sergienko, & Khan, 2022; Jongma et al., 2009; Kulakov & Demchev, 2015; Marsh et al., 2015; Martin & Adcroft, 2010; Merino et al., 2016; Stern et al., 2016) assume that the sea ice force $\vec{F}_{si}$ can be parameterized as a drag force (refer to Equation 2). However, a study conducted by Lichey and Hellmer (2001) that compared modeled and observed trajectories for a tabular iceberg in the Southern Ocean, found that the parameterized sea ice drag force was not enough to reproduce observations at high sea ice concentrations. Therefore, the authors implemented a new parameterization (later modified by Rackow et al., 2017) where $\vec{F}_{si}$ can assume one of three forms, depending on the SIC and strength (which is a function of both SIC and thickness; Hibler, 1979) surrounding the iceberg. In the first case, when SIC is less or equal to 15%, $\vec{F}_{si}$ is set to zero, as at those concentrations the iceberg is considered to be in open water. In the second case, when the SIC is between 15% and 90% (or above 90% but sea ice strength is below a prescribed threshold), $\vec{F}_{si}$ assumes the traditional drag force form. Finally, if sea ice strength is above the prescribed threshold and concentrations are above 90%, the iceberg will not have an acceleration of its own but will, instead, move with the sea ice pack.

This approach was used in a number of studies thereafter (e.g., Condron & Hill, 2021; Eik, 2009; Hunke & Comeau, 2011; Keghouche et al., 2009; Rackow et al., 2017; Wesche & Dierking, 2016), mostly applied to the Southern Ocean, to the Barents Sea, or to paleoclimate studies. Modeling studies that focus on the presence of icebergs in the Grand Banks still assume that $\vec{F}_{si}$ is negligible or is represented as a drag force. Given the aforementioned importance of Baffin Bay's sea ice cover in controlling the iceberg's lifetime and the timing that they get "released" to lower latitudes (Marko et al., 1994, 2014), a more realistic parameterization of $\vec{F}_{si}$ in

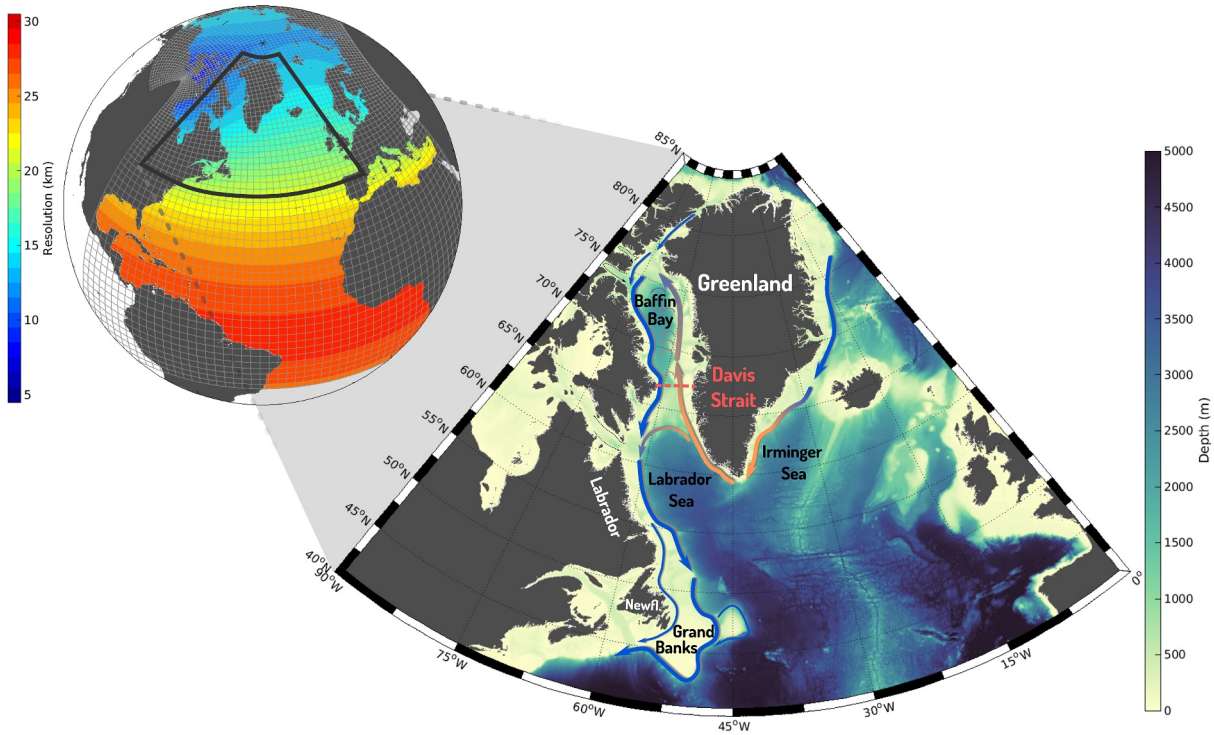

Figure 1. Map showing the bathymetry of most of the subpolar North Atlantic. The locations mentioned in the text are labeled here. The arrows indicate the overall ocean circulation pattern, where orange stands for relatively warm currents, and blue/black for relatively cold currents.

iceberg models used for this region is potentially critical to getting an accurate representation of the intensity of each year's Newfoundland iceberg season and the freshwater distribution associated with iceberg melting.

Here, we implement a modified version of Rackow et al. (2017) "sea ice locking" (SIL) parameterization in the iceberg module of the Nucleus for European Modeling of the Ocean model (NEMO-ICB) to understand its impact on the drift of icebergs through Baffin Bay, a region covered by a dense sea ice pack during winter. The novelty in our approach is that, instead of prescribing a sea ice strength threshold for the entire domain, we calculate it locally for each iceberg, since a lower sea ice strength might be enough to lock the iceberg in a relatively calm environment. We have carried out two NEMO simulations: a control run (CTL) where $\vec{F}_{si}$ is parameterized as a drag force (Marsh et al., 2015), and a "sea ice locking" (SIL) run where $\vec{F}_{si}$ takes one of the three forms described above, based on Lichey and Hellmer (2001) and Rackow et al. (2017). Their outputs, combined with observations of icebergs through satellite imagery (Crawford et al., 2018) and tracking beacons (Garbo & Mueller, 2024), are used to answer the following questions:

1. Is sea ice locking really present in Baffin Bay?
2. How do icebergs in Baffin Bay behave (their speed with respect to sea ice) in a concentrated and strong sea ice pack, when only a sea ice drag force is applied?
3. Do icebergs change their trajectories when the SIL mechanism is present? Are those trajectories realistic?
4. Does SIL better reproduce the variability in the number of icebergs reaching the Grand Banks compared to CTL, without locking?
5. Is the meltwater distribution across the subpolar North Atlantic affected by the implementation of the SIL parameterization?

2. Methods

2.1. NEMO-ICB and the Sea Ice Force Parameterization

The simulations used in this study were carried out with NEMO version 3.6 (Madec & the NEMO team, 2008), where its ocean component was coupled to the Louvain-La-Neuve sea ice model version 2 (Fichefet &

Maqueda, 1997). NEMO v3.6 debuted an iceberg module (NEMO-ICB, Marsh et al., 2015), where icebergs are treated as Lagrangian particles that drift and deteriorate according to the surrounding environmental conditions. To be more precise, the model's particles might contain one or more icebergs depending on their size class — see Martin and Adcroft (2010) for details. In the following text, we use the word "iceberg" even when referring to the model's particles.

As mentioned in the previous section, most models (including the original version of NEMO-ICB) calculate iceberg drift velocity $\left(\vec{V}_{icb}\right)$ by making its acceleration proportional to the sum of all forces $\left(\Sigma\vec{F}\right)$ acting on the iceberg (Equation 1). Among those forces is $\vec{F}_{si}$, generally represented as a drag force of the form (e.g., Bigg et al., 1997; Marsh et al., 2015)

$$\vec{F}_{si} = \frac{1}{2}\rho_{si}c_{si}Wh|\vec{V}_{si} - \vec{V}_{icb}|\left(\vec{V}_{si} - \vec{V}_{icb}\right) \tag{2}$$

where ρ_{si} is the sea ice density (916.7 kg/m^3), c_{si} is the ice drag coefficient (0.9), W is the iceberg width, h is sea ice thickness, and $\vec{V}_{si}$ is the sea ice velocity. Here, we implement the SIL parameterization described by Lichey and Hellmer (2001) and modified by Rackow et al. (2017) in which $\vec{F}_{si}$ will follow one of three cases, depending on the concentration A and strength P of sea ice surrounding the iceberg. In the first case, when SIC at a given iceberg position is less than or equal to 15%, sea ice has no influence on iceberg dynamics, so $\vec{F}_{si}$ is set to zero and the velocity of the iceberg will depend on all the other forces acting on it. The second case follows the traditional sea ice drag force, given by Equation 2, when SIC is above 15% but the iceberg has not been completely "captured" by sea ice yet (i.e., SIC or strength are below the threshold). This brings us to the third case: when the thresholds of SIC and strength are reached, $\vec{F}_{si}$ is equal and opposite to the sum of all other forces acting on the iceberg,

$$\vec{F}_{si} = -\left(\vec{F}_c + \vec{F}_p + \vec{F}_r + \vec{F}_a + \vec{F}_o\right) \tag{3}$$

which means that the iceberg's own acceleration is zero and its velocity is assigned to be equal to the sea ice velocity. As described by Rackow et al. (2017), we also implement a transition zone between cases two and three to avoid a numerical discontinuity. Notice that the SIL parameterization is one-way only: it does not deal with icebergs' impacts on sea ice.

In practice, here is what NEMO-ICB does under the SIL parameterization.

1. The sea ice model (LIM2, in our case) provides NEMO-ICB with SIC A and thickness h at the iceberg location. NEMO-ICB then calculates sea ice strength P, given by Hibler (1979); Lichey and Hellmer (2001):

$$P = P^* h \exp[-20(1-A)] \tag{4}$$

   where P^* is an empirical coefficient that is chosen just for the iceberg module independently of LIM2. In our experiment, we follow previous studies (Lichey & Hellmer, 2001; Rackow et al., 2017) and use 20,000 N/m^2 for P^*, although we acknowledge that this value should be tuned for smaller Arctic icebergs if proper field observations become available.
2. The values ($v = (A|P)$) obtained at the iceberg location are compared with transition values ($v_t = (A_t|P_t)$) and threshold "locking" values ($v_s = (A_s|P_s)$) and a factor α is assigned to that relationship:

$$\alpha_v = \begin{cases} 0 & \text{for} \quad v < v_t \\ \dfrac{v - v_t}{v_t - v_s} & \text{for} \quad v_t \le v \le v_s \\ 1 & \text{for} \quad v > v_s \end{cases} \tag{5}$$

Therefore, we end up with a factor α_A for the comparison between A and A_t, A_s and a factor α_P for the comparison between P and P_t, P_s.

3. A locking coefficient λ is calculated as the product of those two factors:

$$\lambda = \alpha_A \cdot \alpha_P \tag{6}$$

4. If $\lambda > 0$ (i.e., if A and/or P are above the transition values) or if $A \leq 15\%$, then $\vec{F}_{si}$ is set to zero and $\Sigma\vec{F} = \vec{F}_c + \vec{F}_p + \vec{F}_r + \vec{F}_a + \vec{F}_o$; otherwise, $\vec{F}_{si}$ is calculated using Equation 2, and $\Sigma\vec{F} = \vec{F}_c + \vec{F}_p + \vec{F}_r + \vec{F}_a + \vec{F}_o + \vec{F}_{si}$.
5. $\Sigma\vec{F}$ is used to calculate a "preliminary" iceberg velocity $\vec{V}_{\Sigma F}$ using Equation 1. The final iceberg velocity $\vec{V}_{icb}$ will be given by:

$$\vec{V}_{icb} = (1 - \lambda) \cdot \vec{V}_{\Sigma F} + \lambda \cdot \vec{V}_{si} \tag{7}$$

that is, it will be a combination of the velocity generated by the forces acting on the iceberg and the sea ice velocity. Notice that

(a) If $\lambda = 0$, the SIC and strength at the iceberg location is not enough to even start capturing the iceberg; therefore, $\vec{V}_{icb} = \vec{V}_{\Sigma F}$, where sea ice drag might have contributed to that velocity if $A > 15\%$ and ($A < A_t$ or $P < P_t$).

(b) If $0 < \lambda < 1$, $\vec{V}_{icb}$ is partly given by $\vec{V}_{\Sigma F}$ and partly by $\vec{V}_{si}$. This is the transition zone introduced by Rackow et al. (2017). In this case, the influence of sea ice over the iceberg is directly imposed by its velocity (sea ice starts "pushing" the iceberg) rather than acting as a drag force (remember that, when $\lambda > 0$, $\vec{F}_{si} = 0$).

(c) If $\lambda = 1$ then the local SIC and strength have met or surpassed their thresholds and the iceberg gets locked into the sea ice pack, nullifying $\vec{V}_{\Sigma F}$ because in this case we assume that Equation 3 is true, and assigning $\vec{V}_{icb} = \vec{V}_{si}$

This is summarized in Figure 2.

Table 1 shows the threshold values chosen for this study. While 90% SIC is a commonly accepted threshold for icebergs to be locked in the Southern Ocean, and Schodlok et al. (2006) mentions 86% as the SIC at which icebergs start getting locked (which is why $A_t = A_s - 0.04$), those values are arbitrary for the North Atlantic. To determine if those values are appropriate, beacons would need to be deployed on icebergs and surrounding sea ice floes to calculate the deformation of their synchronous trajectories, as done by Schodlok et al. (2006). The novelty in our parameterization comes from the choice of P_s: instead of prescribing it as a constant for the entire domain (13,000 N/m in Lichey and Hellmer (2001) and 10,000 N/m in Rackow et al. (2017)), we calculate it locally as the force (by unit of length) required for sea ice to resist (without breaking) all the other forces imposed on the iceberg. In other words, P_s is equal to $\vec{F}_{si}$ (Equation 3) divided by the iceberg's width. In NEMO-ICB, icebergs orient their length parallel to the currents (Bigg et al., 1997), which makes their width the "bumper" that is facing downstream. We chose to start capturing the iceberg in sea ice once P reaches 80% of P_s (i.e., $P_t = 0.8P_s$) to be consistent with Rackow et al. (2017) — but, again, that is an arbitrary choice and should be calibrated with proper observations.

2.2. Experimental Configurations

Two simulations were used in this study. *CTL* is the control simulation where we use the traditional sea ice-iceberg parametrization, that is, $\vec{F}_{si}$ is a drag force (Equation 2). *SIL* is the simulation where we implemented the SIL parameterization. In all other aspects, the simulations are identical. We used the Arctic and Northern Hemisphere Atlantic (https://canadian-nemo-ocean-modelling-forum-commuity-of-practice.readthedocs.io/en/latest/Institutions/UofA/Configurations/ANHA4/index.html) configuration at 1/4°resolution, with open boundaries in the Bering Strait and at 20°S; hourly atmospheric forcing from the Canadian Meteorological Center's global deterministic prediction system reforecasts (CGRF) at 33 km resolution (G. C. Smith et al., 2014); ocean initial and boundary conditions from GLORYS2v3 (Masina et al., 2017); river runoff forcing from HydroGFD (Stadnyk et al., 2021); and Greenland liquid and solid interannually varying discharge rates from Bamber et al. (2018a). No solid discharge rate are provided for the Canadian Arctic Archipelago; therefore, there are no icebergs of Canadian origin in the simulations. For more details on how the solid discharge is applied to generate

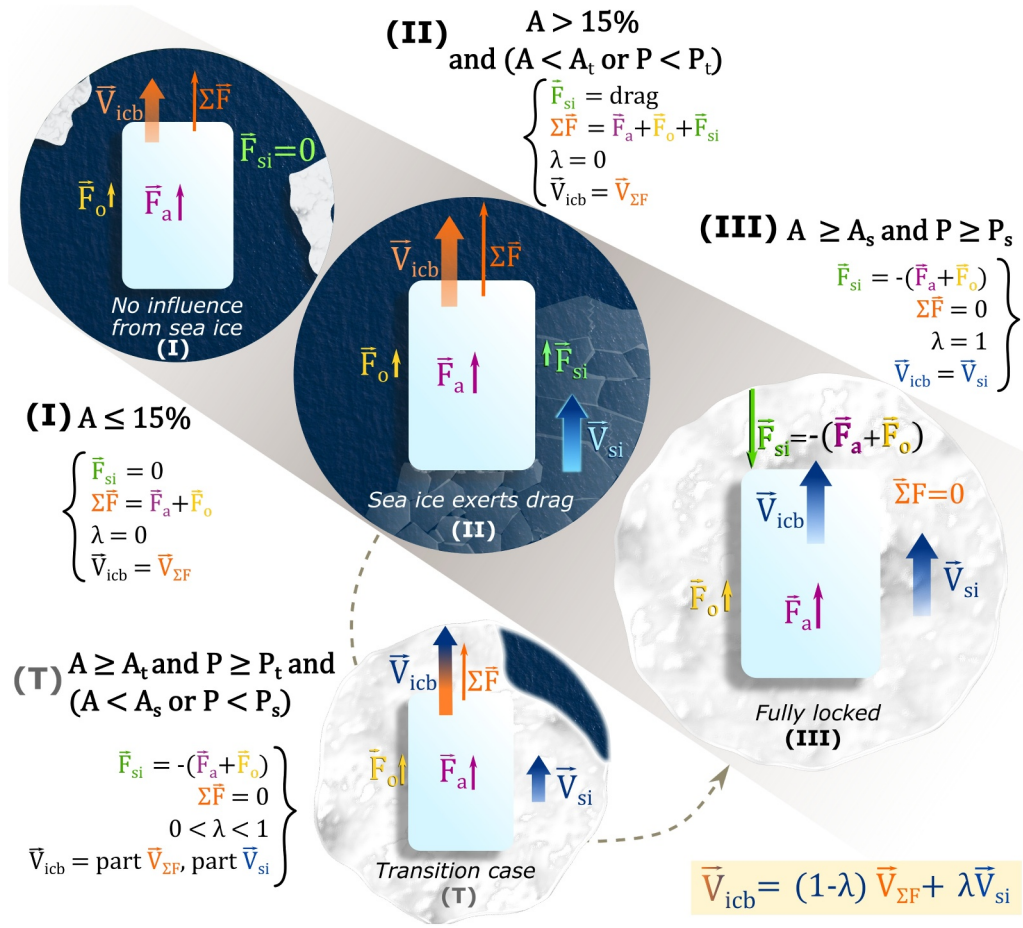

Figure 2. Schematic summarizing the sea ice locking parameterization. $\vec{F}_c$, $\vec{F}_p$, and $\vec{F}_r$ are omitted for simplicity.

icebergs in NEMO, please see Marson et al. (2021). Tides are represented as well, and a passive tracer was linked to iceberg melt to track its overall distribution. Both simulations were run from 2002 to 2017, and outputs from the iceberg module are daily. Ocean and sea ice average fields depicted in the figures exclude the first two years of simulation (2002–2003), when the ocean is still adjusting to the atmospheric forcing.

2.3. The Observations

We use observations of sea ice velocity and concentration, and iceberg trajectories to show if the SIL mechanism can be detected in Baffin Bay, and if our modeled iceberg trajectories look reasonable. In order to compare iceberg velocities with daily sea ice velocities (Section 2.3.1), consistent and high-frequency sampling of iceberg position was needed. Therefore, we use data from tracking beacons, described in Section 2.3.3. To evaluate iceberg trajectories, we also use a larger database where icebergs were tracked via satellite imagery, which is described in Section 2.3.4.

Table 1
Transition (Subscript t) and Threshold (Subscript s) Values of Sea Ice Concentration (A) and Strength (P)

A_s	A_t	P_s	P_t
90%	$A_s - 0.04$	$\vec{F}_{si}/W$	$0.8P_s$

2.3.1. Sea Ice Velocities and Concentration

Sea ice velocities were provided by the *Polar Pathfinder Daily 25 km EASE-Grid Sea Ice Motion Vectors, Version 4* (https://nsidc.org/data/nsidc-0116/versions/4; Tschudi & Univ Of CO, 2019), at a resolution of 25 km. The measurements are obtained by analyzing subsequent satellite images and identifying the same feature (e.g., an ice floe) through spatial correlation. This method is valid for areas with relatively stable sea ice, away from the ice edge. Given the displacement of such features and the time passed between when

Table 2
Characteristics of the Icebergs Tracked With Cryologgers

Iceberg ID	Length (m)	Width (m)	Sail (m)	Date range
5110	269	204	NA	Aug 2018[a] – Jul 2019
5310	700	240	33	May 2020 – Oct 2020
1950	310	300	12	Oct 2021 – Jul 2022

Note. All transmissions from icebergs 5310 and 1950 were hourly. [a]Position transmissions were irregular until 27 Dec 2018, when they became hourly.

the two images were taken, an average velocity can be calculated. Estimates from different sources/instruments are then combined into a daily data set that spans from 1978 to December 2021. Sea ice velocities obtained only from samples over 1,250 km away from the grid point of interest, as well as values too close (within 25 km) to the coastline (which might contain false ice), were flagged and here labeled as "uncertain."

Sea ice concentration was obtained from the data set *ASI Version 5 SIC* (Spreen et al., 2008), which is available at a 6.25 km spatial resolution and daily temporal resolution from 2012 to 2023 (https://data.seaice.uni-bremen.de/amsr2/asi_daygrid_swath/n6250/netcdf/). In this data set, measurements from the Advanced Microwave Scanning Radiometer for EOS (AMSR-E) and from the Advanced Microwave Scanning Radiometer 2 (AMSR2) are processed with the ARTIST (Arctic Radiation and Turbulence Interaction STudy) Sea Ice (ASI) algorithm (Spreen et al., 2008). At 0% SIC, the estimated error is large (25%), but it decreases as concentrations increases, reaching 5.7% at 100% SIC (Melsheimer, 2019). The iceberg distance from the sea ice edge was calculated by taking the distance between the iceberg position and the closest grid point with a SIC smaller than 15%. For both sea ice velocity and concentration, we use the estimate from the grid point closest to the iceberg position in our plots.

2.3.2. Icebergs Crossing 48°N

The International Ice Patrol (IIP) keeps count of how many icebergs cross the 48°N line of latitude southward between October one year and September the next year, since 1900 (https://nsidc.org/data/g10028/versions/1; International Ice Patrol, 2020). This data set is commonly referred to as I48N and serves as a measurement of the presence of icebergs in the Grand Banks, off Newfoundland. The IIP have used a combination of ship reports, visual observations from aircraft, airborne radar and, more recently, satellite imagery to detect those icebergs. Here, we use I48N from 2008 to 2017 to evaluate the last 10 years of both CTL and SIL simulations. Only the last 10 years are considered here because the iceberg field in the model starts empty, and it takes a few years to consistently have icebergs reaching that far south.

2.3.3. Iceberg Trajectories From Tracking Beacons

We have selected three tabular icebergs whose hourly position were tracked with a Cryologger Ice Tracking Beacon (ITB, Garbo & Mueller, 2024). The Cryologger ITB is a low-cost Arduino-based data logging and telemetry platform that uses a Global Navigation Satellite Systems receiver to position itself (Garbo & Mueller, 2024). The IDs we use to identify them (Table 2) are the last 4 digits of their official tags. The beacons were deployed directly on the iceberg surface by a helicopter operating from the *CCGS Amundsen* icebreaker, during which time photos and estimates of the size of each iceberg were recorded. Refer to Table 2 for more details on each tracked iceberg. Although more icebergs tracks were available, those three are the only ones that met our needs: icebergs that drifted (and were not grounded) through regions covered by sea ice, where sea ice velocity was provided and deemed trustworthy (i.e., calculated with close-by measurements and far from the coastline) and where multi-month data sets were available.

2.3.4. Iceberg Distribution From Satellite Imagery

For the iceberg distribution analysis, iceberg positions were provided by the Canadian Ice Island Drift, Deterioration and Detection (CI2D3) database (Desjardins et al., 2018). This database includes over 25,000 ice islands (large tabular icebergs) that were delineated from RADARSAT-1/-2 and Envisat Synthetic Aperture Radar (SAR) scenes from July 2008 to December 2013. Ice islands that calved from Petermann Glacier and other ice tongues in NW Greenland were followed using SAR imagery and digitized into geospatial polygons. All ice islands bigger than 0.25 km^2 in the Eastern Arctic and northeastern Atlantic are included in the data set at a repeat observation frequency ranging from sub-daily to fortnightly (Crawford et al., 2018). Here, we count the number of CI2D3 icebergs observed in each ANHA4 grid cell for each season.

3. Results and Discussion

3.1. Are Sea Ice Locking and Its Effects Realistic for Baffin Bay?

Given that most observations of icebergs getting locked in sea ice have been made in the Southern Ocean, we investigate if the same mechanism occurs in Baffin Bay. We used hourly positions from three tabular icebergs (identified as 5110, 5310, and 1950) obtained with Cryologger ITBs (Garbo & Mueller, 2024), and compared their daily averaged velocities to daily sea ice velocities obtained from the Polar Pathfinder data set (see Sections 2.3.1 and 2.3.3 for more details). Those velocities were put into context with SIC data derived from AMSR-E and AMSR2. Figure 3 shows a map of the icebergs' trajectories, and their velocities in an associated plot.

Iceberg 5110 (Figure 3a1) was tagged in August 2018, but it was mostly grounded until December 2018. When it started moving, the SIC was around 80% but the iceberg was relatively close to the coastline of Devon Island and, consequently, sea ice velocity estimates are flagged as uncertain. From 18 December 2018 to 01 March 2019, the iceberg was surrounded by sea ice (concentration $\geq$90%) and their velocities are significantly correlated: the Pearson correlation coefficient is 0.49 (p-value of 9.8×10^{-6}), but reaches 0.77 (p-value of 10^{-15}) if the iceberg velocity time series lags the sea ice time series by one day. It is likely that this lag exists due to differences in how the daily velocity averages are calculated for the sea ice and the iceberg. Icebergs daily speeds are averages of hourly estimates between midnight of one day and midnight of the next day. Meanwhile, the sea ice motion data set is a product of combined data from seven different sensors and, for most of them, daily sea ice velocity is based on only two observations 24-hr apart — and not necessarily from midnight to midnight.

Between 02 March and 23 April 2019, although the SIC closest to the iceberg is still equal to or above 90%, the iceberg speeds up and seems to move independently of sea ice (the correlation between their velocities is insignificant at 0.08). A number of factors might explain why iceberg and sea ice velocities lose their correlation under high SIC. First, during this period, the iceberg gets progressively closer to the sea ice edge (refer to the purple line in Figure 3a2 and Movie S1). This brings up two issues: (a) SIC estimates close to the sea ice edge have significant uncertainties (Spreen et al., 2008), and (b) sea ice is more likely to be broken and more easily deformed by the iceberg as we approach the edge (200 km or less) due to the increasing influence of waves (Kohout et al., 2014). Another factor that can explain the low correlation between sea ice and iceberg velocities during this period is the occurrence of relatively strong winds at the iceberg position, particularly by the end of March (see Figure S2a in Supporting Information S1). The changing wind direction during that period might also indicate the passage of a storm. Stronger winds not only imply higher waves that are more likely to break sea ice, but also that a higher sea ice strength is needed to lock the iceberg. Unfortunately, there is no sea ice thickness data along this section of the iceberg trajectory (Figure S3a in Supporting Information S1) and ocean currents cannot be estimated when the ocean is ice covered, so we are not able to estimate P or P_s for tagged icebergs. It is also important to highlight that the sea ice motion estimate is taken from the pixel closest to the iceberg position, but they may vary locally given the 25 km resolution.

Iceberg 5310, although apparently traveling through concentrated sea ice in some days of summer 2020, did not show clear signs of being locked (Figure 3b2). The Pearson correlation coefficient between the iceberg and sea ice velocities is 0.38 (p-value of 0.03). Again, the iceberg seems to have traveled very close to the sea ice edge (purple line in Figure 3b2 and Movie S2), where concentration estimates become uncertain and waves start breaking the sea ice into smaller floes. Additionally, since this was in summer, sea ice was likely melting, and melting sea ice is weaker (as inferred by Lichey and Hellmer (2001)), making it harder to lock the iceberg.

Finally, iceberg 1950 seems to have been locked in sea ice between 18 December 2021 to 18 January 2022. Sea ice concentration at this time was equal to or greater than 90%, and ice velocity correlates relatively well with the 1-day-lagged iceberg velocity (0.50 with a p-value of 0.005). From 19 January to 06 April 2022, however, the velocities seem to lose their synchrony, especially in days where the iceberg's distance from the sea ice edge falls below 200 km and when winds picked up between February and March (Figure S2c in Supporting Information S1).

3.2. How Do Icebergs Behave in Strong Sea Ice When Only a Sea Ice Drag Force Is Parameterized?

Recall, from Section 2.1, that we define a strong sea ice pack as one that is capable of withstanding all the forces acting on the embedded iceberg without breaking. In SIL, this strength (P_s) is determined locally for each iceberg at each time step. Since CTL does not go through that calculation, we need to determine an overall P_s value for

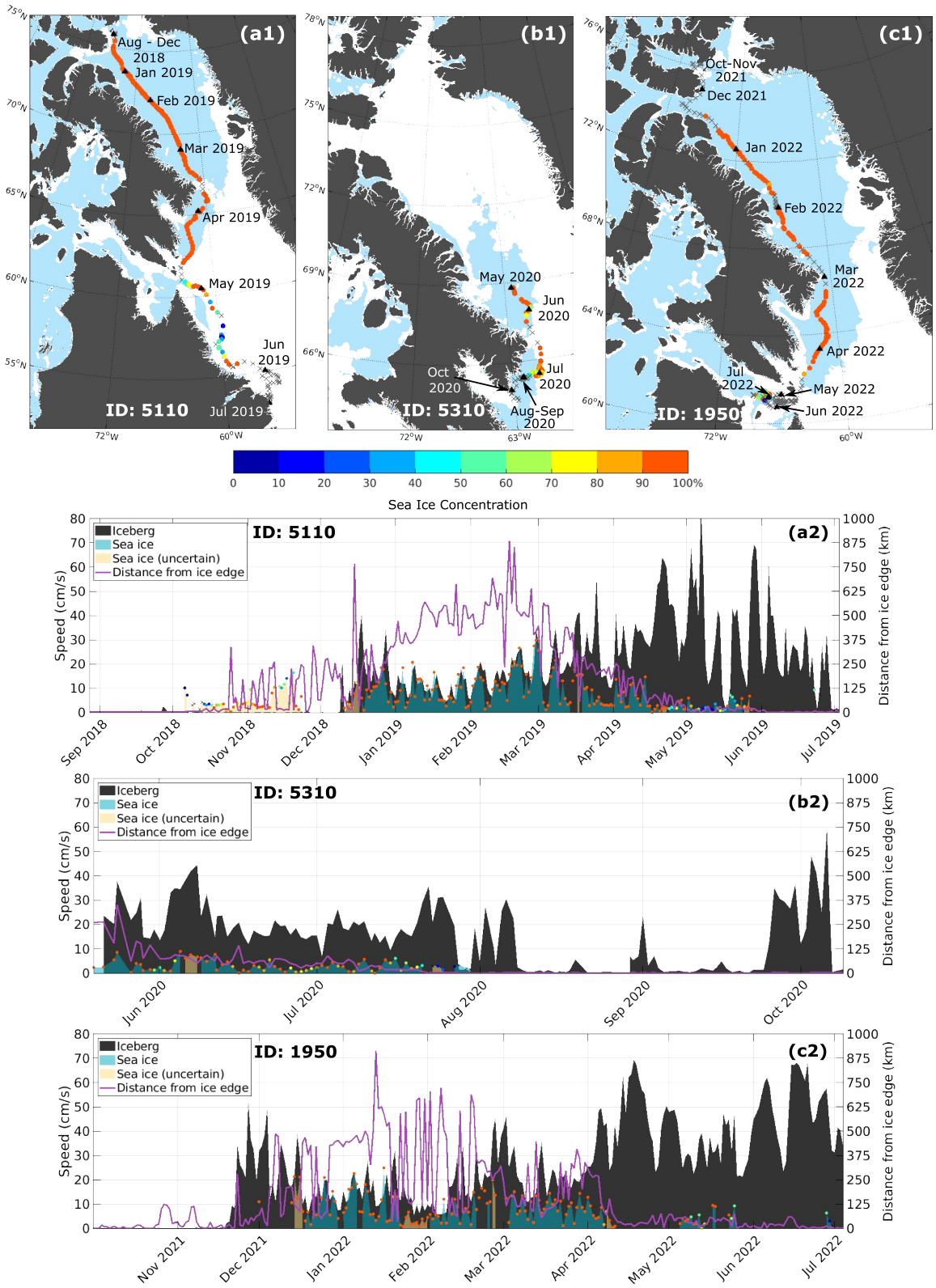

Figure 3.

Baffin Bay above which icebergs would likely be locked, given the Bay's characteristic wind and current speeds. Thus, we follow Lichey and Hellmer (2001) and calculated the sum of F_a and F_o daily for every iceberg in Baffin Bay recorded in CTL, and divide that sum by the iceberg's width W to get to a strength unit (N/m). Most of the time (95% of the instances), $(F_a + F_o)/W$ is smaller than 2,000 N/m (Figure S1 in Supporting Information S1). This means that if sea ice has a strength of 2,000 N/m or more, it will likely lock icebergs in Baffin Bay. This is a significantly lower value compared to the one estimated for the Weddell Sea and used in previous studies: Lichey and Hellmer (2001) found that a sea ice strength threshold of 13,000 N/m allows the model to reproduce an iceberg trajectory better; Rackow et al. (2017) use 10,000 N/m due to the overall lower sea ice concentrations observed in their simulation. It is worth noting, however, that Antarctic icebergs are significantly larger than Greenland icebergs.

Figure 4 shows the CTL relationship between simulated sea ice and iceberg velocities in Baffin Bay in all instances (between 2002 and 2017) when sea ice strength is equal to or greater than 2,000 N/m and SIC is equal to or greater than 90%. The map (Figure 4a) indicates in red where icebergs are, on average, moving faster than sea ice in the model (and blue where they are moving slower). The relationship between those velocities is also pictured in the scatter plot (Figure 4b). Icebergs close to the coastline (especially near northern Greenland) and in northeast Baffin Bay are predicted to move faster than sea ice when the locking mechanism is not implemented (i.e., in the CTL run). On the other hand, icebergs following the Baffin Island Current (BIC) in western Baffin Bay move moderately slower than sea ice. The dashed black line in Figure 4b, which is a linear regression of the individual points, can be compared to the dotted gray line that marks the 1:1 relationship that is parameterized in SIL. It indicates that icebergs predicted to be moving faster than sea ice are more common than slower ones when only a drag force exists between sea ice and iceberg. Therefore, the locking parameterization will mostly act to reduce the velocity of icebergs in the red areas of Figure 4a. Although Lichey and Hellmer (2001) highlight the role of sea ice as a momentum collector from the wind, allowing icebergs to drift at higher speeds when locked within the sea ice pack (which, in Baffin Bay, might happen along the BIC), they also recognize that sea ice can slow down icebergs in certain regions of the Weddell Sea. In general, that seems to happen within strong ocean currents, that is, stronger currents would push icebergs to move faster if there was no sea ice. In our case, however, this seems to be associated only with slower sea ice velocities, which are observed in the weak cyclonic drift in northeast Baffin Bay (Kwok, 2007) and in regions dominated by multiyear sea ice north of Greenland (e.g., Bourke & Garrett, 1987; Moore et al., 2021). Additionally, Figure 4c shows the orientation of iceberg drift in both simulations during winter (January to March). Icebergs in CTL drift westward more often than icebergs in SIL, which move predominantly in the NW–SE axis. This suggests that CTL icebergs tend to follow Baffin Bay's cyclonic circulation more often than icebergs in SIL, which move more markedly southeastward (Figure 5), in line with the bay's orientation. This is because sea ice (and, consequently, locked icebergs) mostly follows the wind stress, which is directed southeastward during winter due to the presence of a persistent sea level pressure trough over Baffin Bay (Kwok, 2007; Tang et al., 2004). When free of sea ice, however, icebergs will tend to follow the geostrophic currents since their keel is affected by the velocity field that goes beyond the Ekman layer (Marson et al., 2018).

3.3. Does the Sea Ice Locking Parameterization Affect the Simulated Distribution of Icebergs in Baffin Bay?

Figure 6 shows the difference in iceberg occurrence between SIL and CTL, that is, how many more (red) or less (blue) icebergs passed through each grid point during the 16 model years in SIL compared to CTL. In general, when sea ice locking is parameterized (SIL), fewer icebergs tend to travel along the Baffin Island shelf break. This is consistent with the idea that, during winter, icebergs will be driven more frequently by sea ice in SIL and by ocean currents in CTL. Therefore, the iceberg distribution differences will reflect the differences between ocean circulation and sea ice motion: while ocean currents tend to concentrate over a narrower area (the BIC, Figure 5a),

Figure 3. (a1) Map showing the trajectory of iceberg 5110. The color of the points indicate daily sea ice concentration (SIC) in the pixel closest to the iceberg at each daily position. Gray points mean no sea ice cover. The blue shading indicates an average SIC ≥90% for Mar–Apr 2019. (a2) Plot showing the iceberg (dark gray) and sea ice (cyan) daily velocities. When sea ice velocity was estimated based on points >1,250 km away and/or too close to the coastline, the value is considered uncertain and is indicated by the yellow shade instead of cyan. Note that cyan and yellow over dark gray shows as teal and brown, respectively. Again, the color of the points on top of the sea ice velocities indicate the SIC closest to where the iceberg was. (b1 and b2, c1 and c2) Same as (a1 and a2), but for icebergs 5310 and 1950, respectively. In panel (b1), the blue shading indicates an average SIC ≥90% for May–Jun 2020; in panel (c1), it indicates an average SIC ≥90% for Feb–Mar 2022.

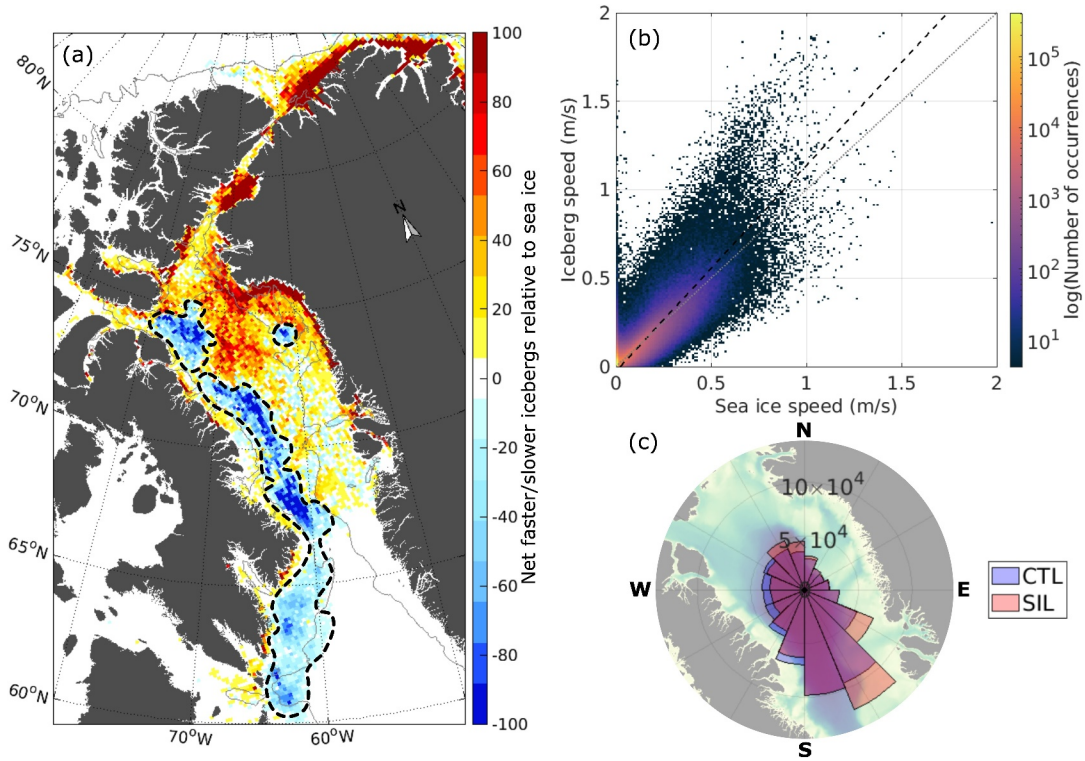

Figure 4. (a) Map showing the net number of icebergs drifting faster (red) or slower (blue) than sea ice (with $P \geq 2{,}000$ N/m) throughout the CTL simulation (2002–2017) in a 1/4° resolution grid. The dashed lines indicates the main regions with slower icebergs. (b) Sea ice versus iceberg speed in strong ($P \geq 2{,}000$ N/m) sea ice pack for the CTL run. Red dots indicate faster icebergs relative to sea ice. The opposite is true for blue dots. The dashed black line shows the linear fit of the blue and red points, while the dotted gray line marks the 1:1 relationship as constrained in the SIL simulation. (c) Direction of icebergs in Baffin Bay during winter (Jan–Mar) in CTL (blue) and SIL (red). The size of the bars indicate the frequency with which icebergs have moved in that direction.

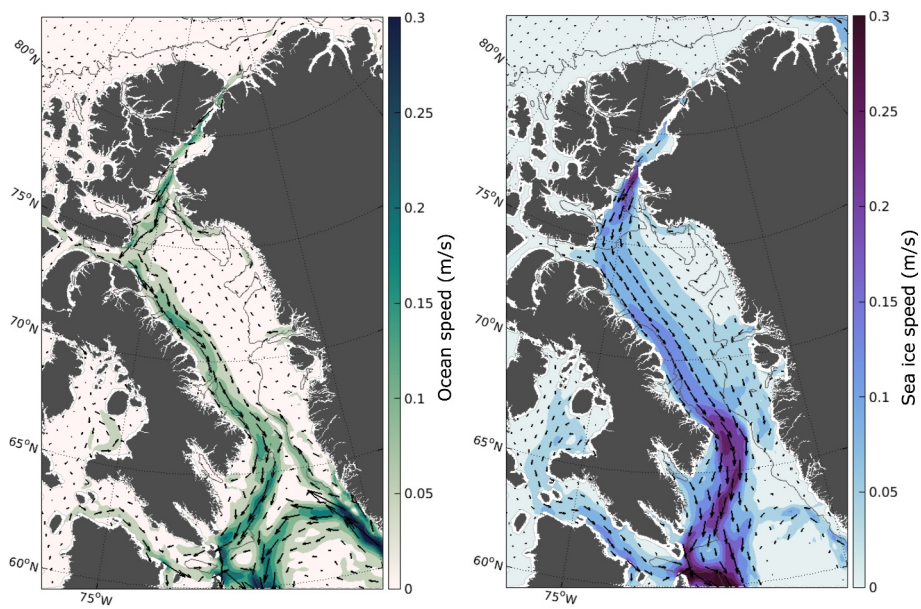

Figure 5. Winter (Jan–Mar) averaged (a) ocean velocities between 0 and 100 m depth, and (b) sea ice velocities in the SIL simulation between 2004 and 2017.

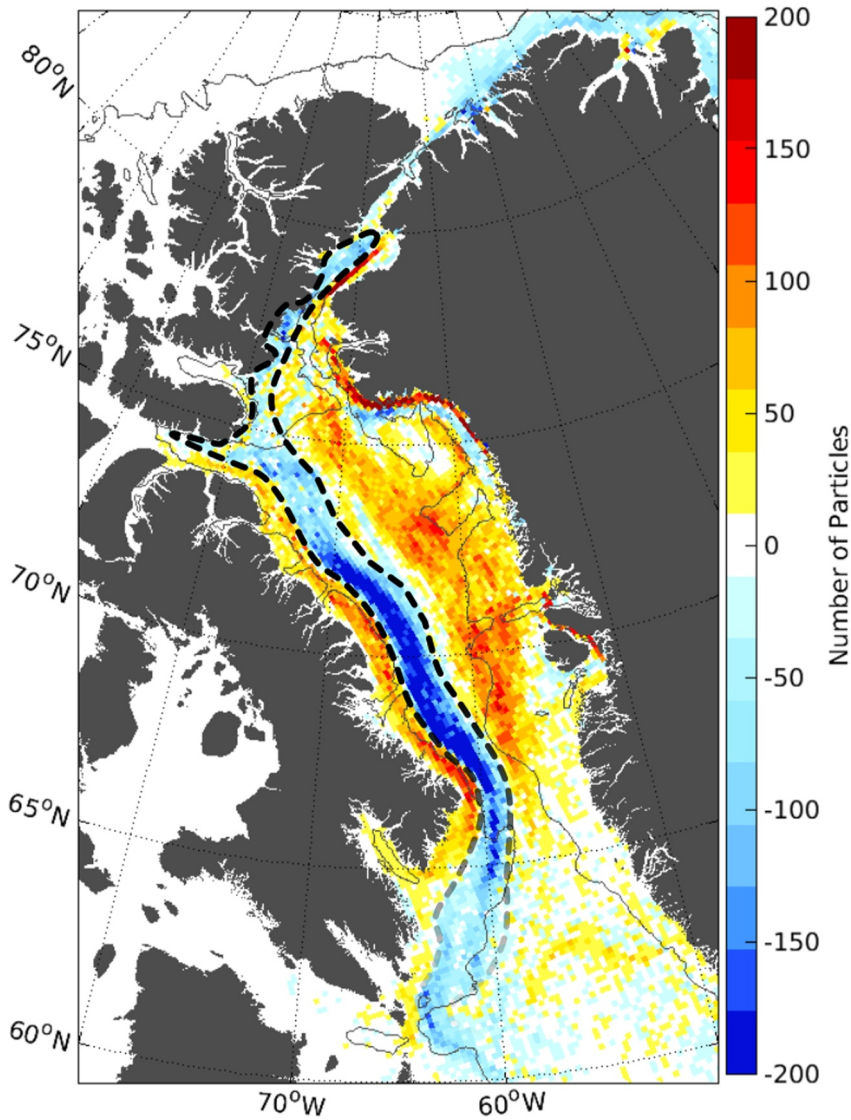

Figure 6. (a) Difference of particle (i.e., cluster of icebergs in the model). occurrence (from January 2002 to December 2017) between SIL and CTL (SIL-CTL), indicating through which grid points the particles drift more (red) or less (blue) when the sea ice locking parameterization is used (SIL) relative to the traditional sea ice-iceberg parameterization (CTL). The dashed black line encircles the main region with negative values.

sea ice tends to move southward more broadly (Figure 5b). Therefore, an iceberg that starts its journey in northwest Greenland during winter is more likely to travel southward away from the Baffin Island shelf break in SIL. Larsen et al. (2015) pointed out that two icebergs drifted southwards in east Baffin Bay between December and February, against the main ocean circulation, and attributed this to the growing winter sea ice. To be clear, that is not to say that icebergs in SIL (or in the real world) never follow that boundary current in winter, as this is very commonly observed — but rather, that they are more likely to deviate from that path when encased in sea ice.

We used the CI2D3 database (Desjardins et al., 2018) to verify if, in the real world, icebergs are more likely to deviate from their BIC trajectory when sea ice is present. We counted the number of icebergs identified in CI2D3 in each ANHA4 grid cell, for each season. Indeed, Figure 7 shows that during winter and spring (top maps) icebergs have a wider distribution across Baffin Bay compared to the almost-ice-free seasons. This supports the idea that icebergs are possibly locked into the sea ice pack, thus following the broader sea ice motion rather than the narrow Baffin Island boundary current (refer to the mean circulation patterns in Figure 5).

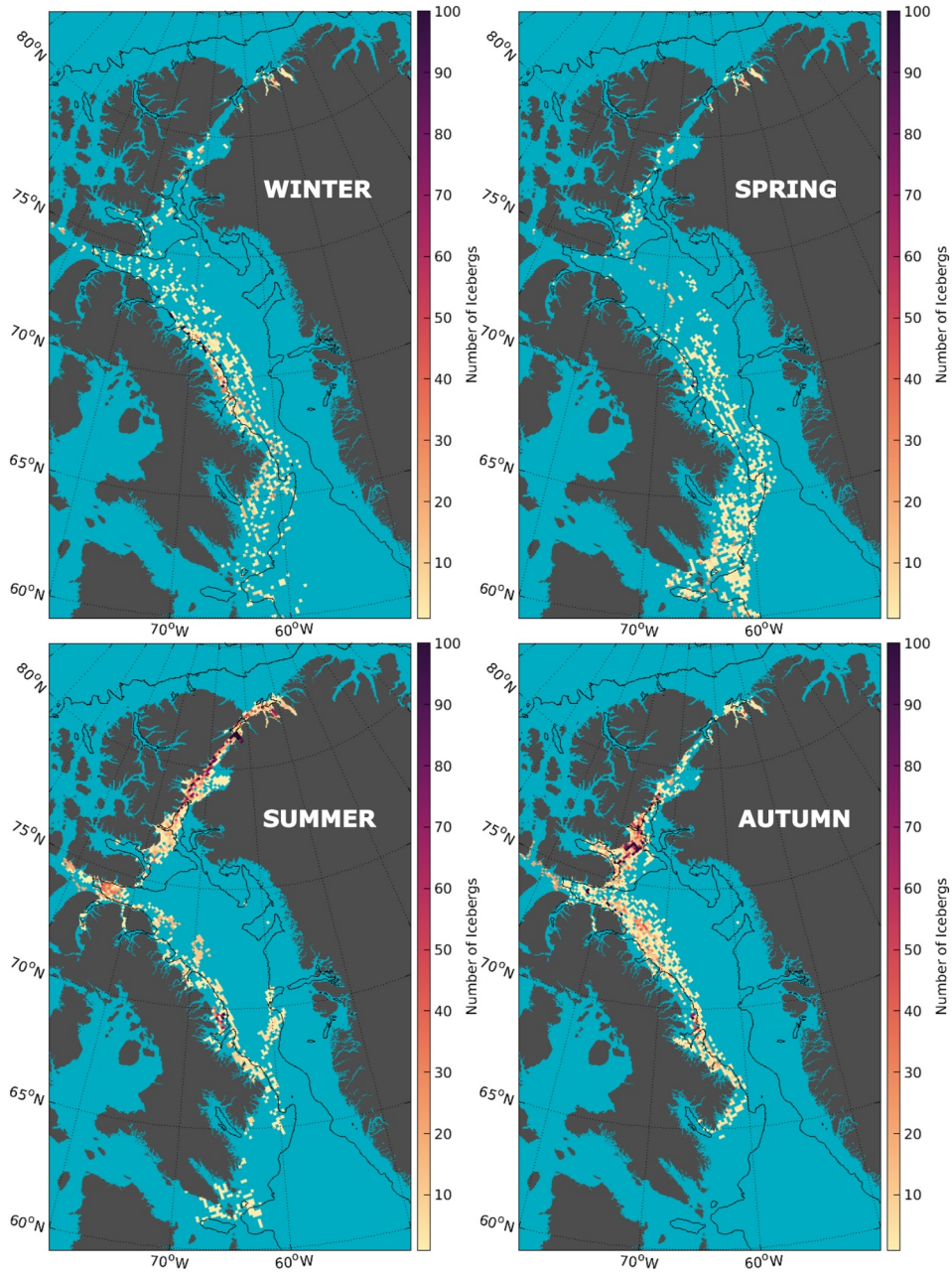

Figure 7. (a) Iceberg occurrence (number per 1/4° × 1/4°gridcell) in the Canadian Ice Island Drift, Deterioration and Detection database for Jan–Mar (upper left), Apr–Jun (upper right), Jul–Sep (lower left), and Oct–Dec (lower right). The black line marks the 500 m isobath for reference.

3.4. Does SIL Better Reproduce the Variability in the Number of Icebergs Reaching the Grand Banks?

The presence of icebergs in the Grand Banks has long been of interest to the U.S. and Canadian Coast Guards, since a large number of transatlantic shipping lanes converge in this region. The seasonal and interannual variability in the number of icebergs crossing 48°N is large and not well understood. Past studies (Marko et al., 1994, 2014) point out that sea ice can be an important driver of this variability. Although the reasons behind I48N variability are not the focus of this study, we use these observations to evaluate our simulations, as was done previously for NEMO-ICB (Marson et al., 2018). Figure 8a shows the average (2008–2017) seasonality of icebergs crossing 48°N from the IIP (dashed line), the CTL simulation (gray bars), and the SIL simulation (teal bars). The sea ice locking parameterization shifted the peak back by 1 month (from May to April), in agreement

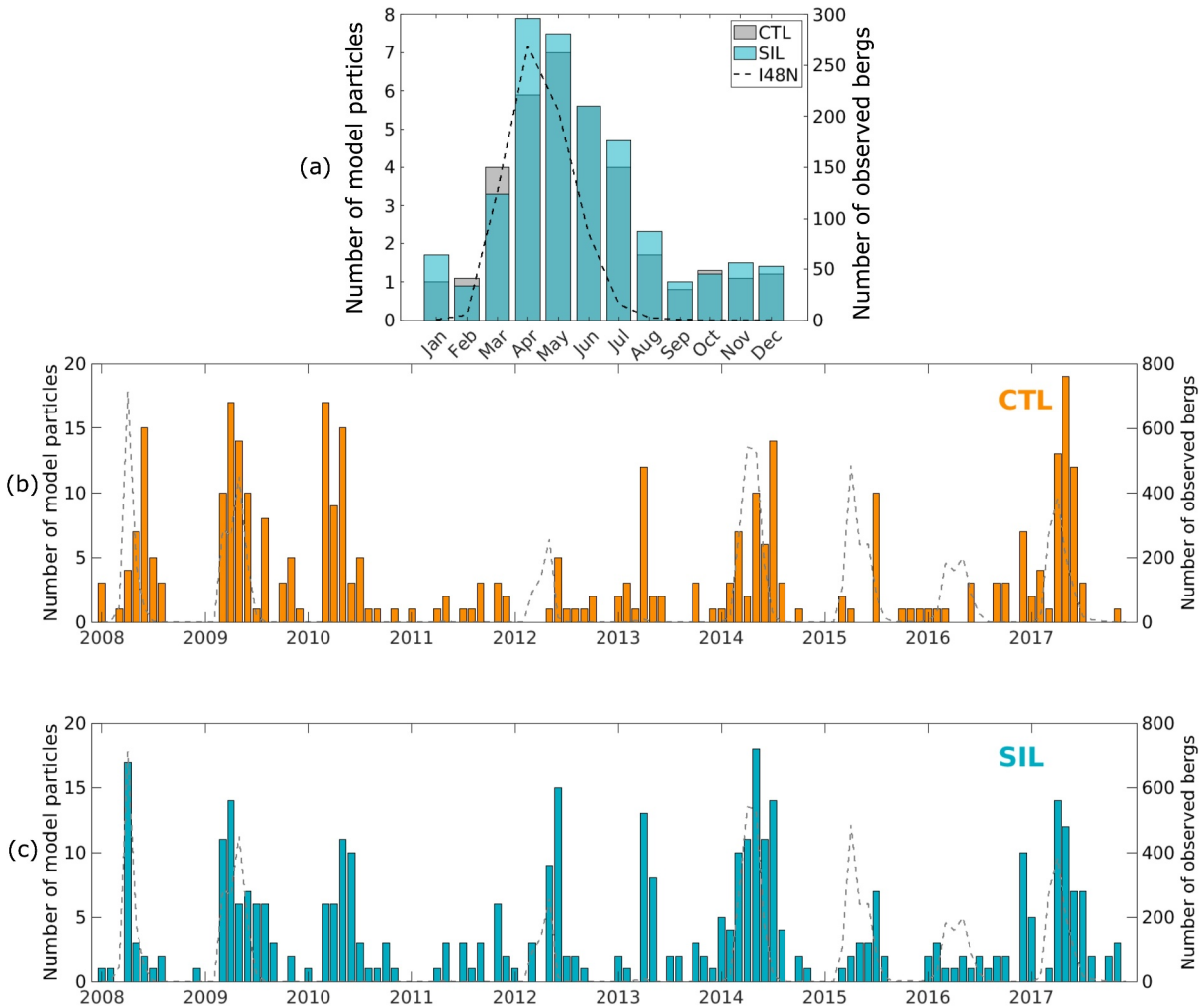

Figure 8. Number of icebergs crossing south of 48°N (a) averaged by month over 2008–2017 in SIL (teal bars), CTL (gray bars), and International Ice Patrol data (dashed line); and (b)–(c) over the years. Notice that the left *y*-axis indicate number of *particles* in the simulations, while the right *y*-axis indicate the number of *icebergs* in I48N. As mentioned in Section 2, modeled particles can carry from 1 to 2,000 icebergs, depending on their size class.

with the peak in observations. It also led to a higher number of icebergs crossing 48°N (390 in total in SIL vs. 347 in total in CTL), which may be linked to a longer lifetime (average of 241 days in SIL vs. 220 days in CTL) provided by the protective nature of sea ice on icebergs (e.g., King & Turnbull, 2022).

Figure 8b shows the interannual variability in the number of icebergs crossing south of 48°N. The SIL parameterization improves the representation of iceberg presence in the Grand Banks by increasing the correlation between modeled and observed I48N from 0.33 (p-value of 2.0×10^{-4}) to 0.56 (p-value of 2.2×10^{-11}). It is clear, nonetheless, that the model has a lot of room for improvement in this metric; the "iceberg season" length should be shorter and the number of icebergs crossing 48°N outside of that season should go to zero. We believe that this can be addressed, at least partly, by adding another iceberg deterioration parameterization in NEMO-ICB known as the "footloose mechanism" (Wagner et al., 2014). This mechanism comes into play when, after waves erode a notch onto the side of the iceberg and the overhanging slab collapses, the remaining underwater "foot" leads to internal stresses caused by its buoyancy. When this stress reaches a critical level, the foot breaks, contributing to a faster iceberg mass loss. Huth, Adcroft, and Sergienko (2022) showed that, by adding the footloose mechanism into their model, they were able to limit the iceberg spatial spread to more realistic ranges. This could translate into a lower iceberg count at the Grand Banks, especially during winter.

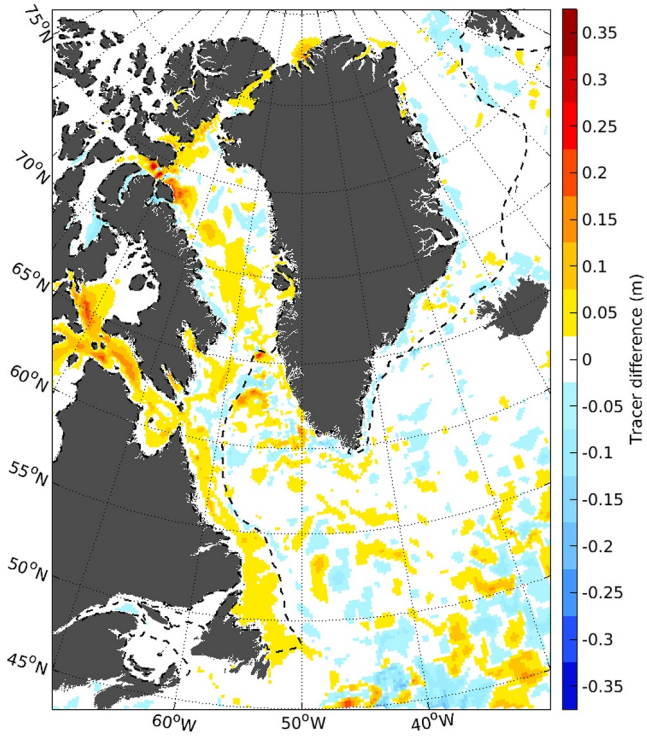

Figure 9. Difference in the final distribution of iceberg meltwater tracer between SIL and CTL (SIL-CTL). The dashed black line marks the March average (2004–2017) sea ice extent (15% isoline in sea ice concentration) in the SIL simulation.

3.5. Is the Iceberg Meltwater Distribution Affected by the Implementation of the SIL Parameterization?

In both simulations, we have inserted a passive tracer in the iceberg melt in order to track its dispersal. Figure 9 represents the difference in the final (31 December 2017) distribution of this tracer, where positive values indicate more iceberg meltwater in SIL, and negative values indicate more iceberg meltwater in CTL. For reference, maximum values of tracer accumulation in a single cell (1/4° × 1/4°) are around 1.8 m. It seems that, when we represent sea ice locking, iceberg melt tends to accumulate in the western side of Baffin Bay, especially near Lancaster Sound, Hudson Strait (where differences can reach 15% of the maximum tracer accumulation), and the Newfoundland and Labrador shelves. In CTL, iceberg melt seems to disperse more into the interior of Baffin Bay and the Labrador Sea. This might be the result of keeping icebergs where sea ice is present (indicated by the black dashed line in Figure 9), instead of allowing them to drift independently of the sea ice pack. As this region is characterized by a negative surface freshwater flux from other sources (likely due to the predominance of sea ice formation; see Figure 3 from Marsh et al., 2015), the additional iceberg melt could be relevant for local freshwater budgets. The sea ice locking mechanism, therefore, can play a role — even if small — in keeping the iceberg meltwater away from the interior of the Labrador (Marson et al., 2021) and Irminger Seas, where it could interfere with deep convection processes (e.g., Böning et al., 2016).

4. Conclusions

In this study, we implemented a parameterization known as "sea ice locking" (Lichey & Hellmer, 2001; Rackow et al., 2017) into the iceberg module of NEMO. We further improved the existing applications of such parameterization by calculating the sea ice strength threshold (the force necessary to oppose all other forces exerted over an iceberg without breaking) locally, instead of using a single value as a parameter for the entire model domain. Below, we summarize our findings regarding the questions we posed in the beginning of this paper:

1. **Is sea ice locking really present in Baffin Bay?**
   Considering the uncertainties associated with observations taken at different resolutions, icebergs appear to move at the same speed as sea ice when it is embedded in a concentrated pack. Situations when such synchrony was not observed include instances where the iceberg approached the sea ice edge, during the melting season, and/or when strong winds and possibly storms took place at the iceberg location.
2. **How do icebergs in Baffin Bay behave (their speed with respect to sea ice) in a concentrated and strong sea ice pack when only a sea ice drag force is applied?**
   When the sea ice force on icebergs is parameterized as a simple drag, simulated icebergs tend to "plow through" a strong sea ice pack, except in the area dominated by the BIC, where sea ice tends to move faster. The direction icebergs take mostly follows the cyclonic circulation of the bay.
3. **Do the icebergs change their trajectories when the SIL mechanism is present? Are those trajectories realistic?**
   Modeled icebergs still travel within the BIC, but do so less often during winter. When sea ice is present in elevated concentrations and strength, icebergs are more likely to travel southeastward away from the current boundaries when the SIL mechanism is considered. The distribution of icebergs obtained from satellite in summer/fall versus winter/spring supports this finding.
4. **Does SIL better reproduce the variability in the number of icebergs reaching the Grand Banks compared to CTL?**
   SIL does a better job of reproducing the seasonality of iceberg occurrence south of 48°N ($r = 0.56$) than CTL ($r = 0.33$), especially regarding the timing of the seasonal peak. However, the model still needs

improvement in the off-season, when no icebergs should be reaching the Grand Banks, according to observations.

5. **Is the meltwater distribution through the subpolar North Atlantic affected by the implementation of the SIL parameterization?**

   While most differences are small and can be attributed to a randomness inherent to each numerical simulation, there seems to be a tendency of iceberg melt accumulation toward the Canadian continental shelves in SIL as opposed to a more widespread distribution in CTL.

We highlight that the calibration of the thresholds is important. Eik (2009) used the Lichey and Hellmer (2001) parameterization for modeling iceberg drift in the Barents Sea, but pointed out that the modeled trajectory did not match the observed drift. The author speculated that the sea ice drift itself may be poorly represented or that the sea ice locking parameterization may be unsuitable for the region. However, they used a low P_s threshold of 660 N/m, and we have not found an analysis that shows that this strength threshold is appropriate for the Barents Sea. On the same note, here we point out the limitations of our study:

- Although we have used a SIC threshold of 90%, the real-world data available is not enough to indicate if this value is appropriate for Baffin Bay. Schodlok et al. (2006) mention that this threshold is variable and dependent on the location. Therefore, more field observations are needed to determine suitable regional values of this threshold.
- Additional sensitivity experiments with varied P^* values are also recommended, particularly for areas/periods of melting sea ice where P^* seems to be lower (Lichey & Hellmer, 2001).
- Grounding of icebergs is not properly handled in NEMO yet, as icebergs only slow down in shallow areas (Merino et al., 2016). Grounding might override the sea ice locking mechanism in certain situations (Yulmetov et al., 2016).
- The drag force of sea ice on "unlocked" icebergs (case II in Figure 2) is not dependent on SIC (which ranges from 15% to 86% in that case). This is likely not realistic (Zeinali Torbati et al., 2020) and a new parameterization of the sea ice drag force should be developed to include a dependency on SIC.

The sea ice locking of icebergs appears to be a realistic process according to existing observations and literature reports. Although focused measurements of SIC, thickness, velocity, and iceberg speed in Baffin Bay are warranted, we are confident that the implementation of such parameterization in NEMO is an improvement over the original drag-only sea ice-iceberg force.

Acknowledgments

J. Marson would like to thank Dr. Thomas Rackow for sharing his sea ice locking code implemented in FESOM. The authors gratefully acknowledge the financial and logistic support of grants from the Natural Sciences and Engineering Research Council of Canada (RGPIN-2021-02921, RGPIN-04357, RGPIN-2017-06020, and RGPCC-433898), ArcticNet Network of Centres of Excellence Canada, Amundsen Science, Canadian Ice Service, University of Ottawa, as well as Polar Knowledge Canada (PKC-NST-1617-0003). J. Marson thanks MEOPAR for the financial support through the Postdoctoral Award program (PDF-9-2018) and University of Alberta's Earth and Atmospheric Sciences department support through the Postdoctoral position in the Climate of the Canadian North. The authors are grateful to the NEMO development team and the Drakkar project for providing the model and continuous guidance, and to the Digital Research Alliance of Canada for computational resources. The authors would also like to thank G. Smith and G. Garric for the model inputs. Finally, we thank the editors and anonymous referees for their helpful suggestions.

Data Availability Statement

The relevant outputs from SIL and CTL simulations are available at the Canadian Watershed Information Network (CanWIN): https://canwin-datahub.ad.umanitoba.ca/data/dataset/nemo-anha4-seaice-locking-icebergs (Marson, 2023). The newest version of NEMO (v4.2.2) is available for download at https://forge.nemo-ocean.eu/nemo/nemo/-/releases/4.2.2 (The NEMO Team, 2024). Greenland freshwater flux data analyzed in this study is presented in Bamber et al. (2018a) and is available at https://www.bodc.ac.uk/ (Bamber et al., 2018b).

References

Andersson, L. E., Scibilia, F., & Imsland, L. (2016). An estimation-forecast set-up for iceberg drift prediction. *Cold Regions Science and Technology*, *131*, 88–107. https://doi.org/10.1016/j.coldregions.2016.08.001

Bamber, J. L., Tedstone, A. J., King, M. D., Howat, I. M., Enderlin, E. M., Van Den Broeke, M. R., & Noel, B. (2018a). Land ice freshwater budget of the Arctic and North Atlantic Oceans: 1. Data, methods, and results. *Journal of Geophysical Research: Oceans*, *123*(3), 1827–1837. https://doi.org/10.1002/2017JC013605

Bamber, J. L., Tedstone, A. J., King, M. D., Howat, I. M., Enderlin, E. M., Van Den Broeke, M. R., & Noel, B. P. Y. (2018b). Modelled and observational freshwater flux time series for land ice in the Arctic and North Atlantic for 1958–2016 [Dataset]. British Oceanographic Data Centre, Natural Environment Research Council. https://doi.org/10.5285/643AA9BC-BCD6-45AD-E053-6C86ABC07DA0

Bigg, G. R., Cropper, T. E., O'Neill, C. K., Arnold, A. K., Fleming, A. H., Marsh, R., et al. (2018). A model for assessing iceberg hazard. *Natural Hazards*, *92*(2), 1113–1136. https://doi.org/10.1007/s11069-018-3243-x

Bigg, G. R., Jutard, Q., & Marsh, R. (2021). Evidence for iceberg fertilization of the NW Atlantic (Preprint). https://doi.org/10.5194/os-2021-61

Bigg, G. R., Wadley, M. R., Stevens, D. P., & Johnson, J. A. (1996). Prediction of iceberg trajectories for the North Atlantic and Arctic oceans. *Geophysical Research Letters*, *23*(24), 3587–3590. https://doi.org/10.1029/96GL03369

Bigg, G. R., Wadley, M. R., Stevens, D. P., & Johnson, J. A. (1997). Modelling the dynamics and thermodynamics of icebergs. *Cold Regions Science and Technology*, *26*(2), 113–135. https://doi.org/10.1016/S0165-232X(97)00012-8

Böning, C. W., Behrens, E., Biastoch, A., Getzlaff, K., & Bamber, J. L. (2016). Emerging impact of Greenland meltwater on deepwater formation in the North Atlantic Ocean. *Nature Geoscience*, *9*(7), 523–527. https://doi.org/10.1038/ngeo2740

Bourke, R. H., & Garrett, R. P. (1987). Sea ice thickness distribution in the Arctic Ocean. *Cold Regions Science and Technology*, *13*(3), 259–280. https://doi.org/10.1016/0165-232X(87)90007-3

Condron, A., & Hill, J. C. (2021). Timing of iceberg scours and massive ice-rafting events in the subtropical North Atlantic. *Nature Communications*, *12*(1), 3668. https://doi.org/10.1038/s41467-021-23924-0

Crawford, A., Crocker, G., Mueller, D., Desjardins, L., Saper, R., & Carrieres, T. (2018). The Canadian ice island drift, deterioration and detection (CI2D3) database. *Journal of Glaciology*, *64*(245), 517–521. https://doi.org/10.1017/jog.2018.36

Desjardins, L., Crawford, A., Mueller, D., Saper, R., Schaad, C., Stewart-Jones, E., & Shepherd, J. (2018). Canadian ice island drift, deterioration and detection database (CI2D3 database). *Canadian Cryospheric Information Network*. https://doi.org/10.21963/12678

Ding, Y., Mu, C., Wu, T., Hu, G., Zou, D., Wang, D., et al. (2021). Increasing cryospheric hazards in a warming climate. *Earth-Science Reviews*, *213*, 103500. https://doi.org/10.1016/j.earscirev.2020.103500

Eik, K. (2009). Iceberg drift modelling and validation of applied metocean hindcast data. *Cold Regions Science and Technology*, *57*(2), 67–90. https://doi.org/10.1016/j.coldregions.2009.02.009

El-Tahan, H., Venkatesh, S., & El-Tahan, M. (1988). Evaluation of a model for predicting the drift of iceberg ensembles. *Journal of Offshore Mechanics and Arctic Engineering*, *110*(2), 172–179. https://doi.org/10.1115/1.3257047

England, M. R., Wagner, T. J. W., & Eisenman, I. (2020). Modeling the breakup of tabular icebergs. *Science Advances*, *6*(51), eabd1273. https://doi.org/10.1126/sciadv.abd1273

Fichefet, T., & Maqueda, M. A. M. (1997). Sensitivity of a global sea ice model to the treatment of ice thermodynamics and dynamics. *Journal of Geophysical Research*, *102*(C6), 12609–12646. https://doi.org/10.1029/97JC00480

Garbo, A., & Mueller, D. (2024). Cryologger ice tracking Beacon: A low-cost, open-source platform for tracking icebergs and ice islands. *Sensors*, *24*(4), 1044. https://doi.org/10.3390/s24041044

Gladstone, R. M., Bigg, G. R., & Nicholls, K. W. (2001). Iceberg trajectory modeling and meltwater injection in the Southern Ocean. *Journal of Geophysical Research*, *106*(C9), 19903–19915. https://doi.org/10.1029/2000JC000347

Hersbach, H., Bell, B., Berrisford, P., Biavati, G., Horányi, A., Muñoz Sabater, J., et al. (2018). ERA5 hourly data on single levels from 1940 to present. Copernicus Climate Change Service (C3S) Climate Data Store (CDS). https://doi.org/10.24381/cds.adbb2d47

Hersbach, H., Bell, B., Berrisford, P., Hirahara, S., Horányi, A., Muñoz-Sabater, J., et al. (2020). The ERA5 global reanalysis. *Quarterly Journal of the Royal Meteorological Society*, *146*(730), 1999–2049. https://doi.org/10.1002/qj.3803

Hibler, W. D. (1979). A dynamic thermodynamic Sea Ice Model. *Journal of Physical Oceanography*, *9*(4), 815–846. https://doi.org/10.1175/1520-0485(1979)009⟨0815:ADTSIM⟩2.0.CO;2

Hill, B. T. (2006). Ship collision with iceberg database. In *Day 3 Tue, July 18, 2006*. SNAME. D031S008R002. https://doi.org/10.5957/ICETECH-2006-117

Hopwood, M. J., Carroll, D., Höfer, J., Achterberg, E. P., Meire, L., Le Moigne, F. A. C., et al. (2019). Highly variable iron content modulates iceberg-ocean fertilisation and potential carbon export. *Nature Communications*, *10*(1), 5261. https://doi.org/10.1038/s41467-019-13231-0

Hunke, E. C., & Comeau, D. (2011). Sea ice and iceberg dynamic interaction. *Journal of Geophysical Research*, *116*(C5), C05008. https://doi.org/10.1029/2010JC006588

Huth, A., Adcroft, A., & Sergienko, O. (2022). Parameterizing tabular-iceberg decay in an Ocean Model. *Journal of Advances in Modeling Earth Systems*, *14*(3), e2021MS002869. https://doi.org/10.1029/2021MS002869

Huth, A., Adcroft, A., Sergienko, O., & Khan, N. (2022). Ocean currents break up a tabular iceberg. *Science Advances*, *8*(42), eabq6974. https://doi.org/10.1126/sciadv.abq6974

International Ice Patrol. (2020). International ice Patrol annual count of icebergs south of 48 degrees north, 1900 to present. *NSIDC*. https://doi.org/10.7265/Z6E8-3027

Jongma, J. I., Driesschaert, E., Fichefet, T., Goosse, H., & Renssen, H. (2009). The effect of dynamic–thermodynamic icebergs on the Southern Ocean climate in a three-dimensional model. *Ocean Modelling*, *26*(1), 104–113. https://doi.org/10.1016/j.ocemod.2008.09.007

Keghouche, I., Bertino, L., & Lisæter, K. A. (2009). Parameterization of an iceberg drift model in the Barents Sea. *Journal of Atmospheric and Oceanic Technology*, *26*(10), 2216–2227. https://doi.org/10.1175/2009JTECHO678.1

Keghouche, I., Counillon, F., & Bertino, L. (2010). Modeling dynamics and thermodynamics of icebergs in the Barents Sea from 1987 to 2005. *Journal of Geophysical Research*, *115*(C12), 2010JC006165. https://doi.org/10.1029/2010JC006165

King, T., & Turnbull, I. D. (2022). The changing iceberg regime and links to past and future climate change offshore Newfoundland and Labrador. *The Journal of Ocean Technology*, *17*(3), 39–60.

Kochtitzky, W., Copland, L., Van Wychen, W., Hock, R., Rounce, D. R., Jiskoot, H., et al. (2022). Progress toward globally complete frontal ablation estimates of marine-terminating glaciers. *Annals of Glaciology*, *63*(87–89), 143–152. https://doi.org/10.1017/aog.2023.35

Kohout, A. L., Williams, M. J. M., Dean, S. M., & Meylan, M. H. (2014). Storm-induced sea-ice breakup and the implications for ice extent. *Nature*, *509*(7502), 604–607. https://doi.org/10.1038/nature13262

Kubat, I., Sayed, M., & Savage, S. B. (2005). An operational model of iceberg drift. *International Journal of Offshore and Polar Engineering*, *15*(2).

Kulakov, M. Y., & Demchev, D. M. (2015). Simulation of iceberg drift as a component of ice monitoring in the West Arctic. *Russian Meteorology and Hydrology*, *40*(12), 807–813. https://doi.org/10.3103/S1068373915120055

Kwok, R. (2007). Baffin Bay ice drift and export: 2002–2007. *Geophysical Research Letters*, *34*(19), L19501. https://doi.org/10.1029/2007GL031204

Larsen, P.-H., Hansen, M. O., Buus-Hinkler, J., Krane, K. H., & Sønderskov, C. (2015). Field tracking (GPS) of ten icebergs in eastern Baffin Bay, offshore Upernavik, northwest Greenland. *Journal of Glaciology*, *61*(227), 421–437. https://doi.org/10.3189/2015JoG14J216

Lichey, C., & Hellmer, H. H. (2001). Modeling giant-iceberg drift under the influence of sea ice in the Weddell Sea, Antarctica. *Journal of Glaciology*, *47*(158), 452–460. https://doi.org/10.3189/172756501781832133

Løset, S. (1993). Thermal energy conservation in icebergs and tracking by temperature. *Journal of Geophysical Research*, *98*(C6), 10001–10012. https://doi.org/10.1029/93JC00138

Madec, G., & the NEMO team. (2008). *NEMO ocean engine* (Vol. 27). Institut Pierre-Simon Laplace (IPSL). Note du Pole de modelisation.

Marko, J. R., Fissel, D. B., Martinez De Saavedra Alvarez, M., Ross, E., & Kerr, R. (2014). Iceberg severity off the east coast of North America in relation to upstream sea ice variability: An update. In *2014 oceans – St. John's* (pp. 1–6). IEEE. https://doi.org/10.1109/OCEANS.2014.7003128

Marko, J. R., Fissel, D. B., Wadhams, P., Kelly, P. M., & Brown, R. D. (1994). Iceberg severity of eastern North America: Its relationship to Sea Ice variability and climate change. *Journal of Climate*, *7*(9), 1335–1351. https://doi.org/10.1175/1520-0442(1994)007⟨1335:ISOENA⟩2.0.CO;2

Marsh, R., Ivchenko, V. O., Skliris, N., Alderson, S., Bigg, G. R., Madec, G., et al. (2015). NEMO–ICB (v1.0): Interactive icebergs in the NEMO ocean model globally configured at eddy-permitting resolution. *Geoscientific Model Development*, *8*(5), 1547–1562. https://doi.org/10.5194/gmd-8-1547-2015

Marson, J. M. (2023). NEMO-ANHA4 Sea ice locking of icebergs [Dataset]. *CanWIN*. https://doi.org/10.34992/mq60-c722

Marson, J. M., Gillard, L. C., & Myers, P. G. (2021). Distinct Ocean responses to Greenland's liquid runoff and iceberg melt. *Journal of Geophysical Research: Oceans*, *126*(12). https://doi.org/10.1029/2021JC017542

Marson, J. M., Myers, P. G., Hu, X., & Le Sommer, J. (2018). Using vertically integrated ocean fields to characterize Greenland icebergs' distribution and lifetime. *Geophysical Research Letters*, *45*(9), 4208–4217. https://doi.org/10.1029/2018GL077676

Martin, T., & Adcroft, A. (2010). Parameterizing the fresh-water flux from land ice to ocean with interactive icebergs in a coupled climate model. *Ocean Modelling*, *34*(3–4), 111–124. https://doi.org/10.1016/j.ocemod.2010.05.001

Masina, S., Storto, A., Ferry, N., Valdivieso, M., Haines, K., Balmaseda, M., et al. (2017). An ensemble of eddy-permitting global ocean reanalyses from the MyOcean project. *Climate Dynamics*, *49*(3), 813–841. https://doi.org/10.1007/s00382-015-2728-5

Melsheimer, C. (2019). *ASI version 5 Sea Ice concentration user guide*. (Version V0.9.2). Institute of Environmental Physics, University of Bremen.

Merino, N., Le Sommer, J., Durand, G., Jourdain, N. C., Madec, G., Mathiot, P., & Tournadre, J. (2016). Antarctic icebergs melt over the Southern Ocean: Climatology and impact on sea ice. *Ocean Modelling*, *104*, 99–110. https://doi.org/10.1016/j.ocemod.2016.05.001

Moore, G. W. K., Howell, S. E. L., Brady, M., Xu, X., & McNeil, K. (2021). Anomalous collapses of Nares Strait ice arches leads to enhanced export of Arctic sea ice. *Nature Communications*, *12*(1), 1. https://doi.org/10.1038/s41467-020-20314-w

Morison, J., & Goldberg, D. (2012). A brief study of the force balance between a small iceberg, the ocean, sea ice, and atmosphere in the Weddell Sea. *Cold Regions Science and Technology*, *76–77*, 69–76. https://doi.org/10.1016/j.coldregions.2011.10.014

Mountain, D. (1980). On predicting iceberg drift. *Cold Regions Science and Technology*, *1*(3–4), 273–282. https://doi.org/10.1016/0165-232X(80)90055-5

Parayil, J., Demirov, E., & Afanasyev, Y. D. (2022). Effects of wind, waves, and currents on icebergs and surface floats in the Labrador sea: A modeling study. *Journal of Marine Science and Engineering*, *10*(9), 1167. https://doi.org/10.3390/jmse10091167

Peterson, I. K., Prinsenberg, S. J., Pittman, M., & Desjardins, L. (2009). The drift of an exceptionally-large ice island from the Petermann Glacier in 2008. In *Proceedings of the international conference on port and ocean engineering under Arctic conditions*.

Rackow, T., Wesche, C., Timmermann, R., Hellmer, H. H., Juricke, S., & Jung, T. (2017). A simulation of small to giant Antarctic iceberg evolution: Differential impact on climatology estimates. *Journal of Geophysical Research: Oceans*, *122*(4), 3170–3190. https://doi.org/10.1002/2016JC012513

Ricker, R., Hendricks, S., Kaleschke, L., Tian-Kunze, X., King, J., & Haas, C. (2017). A weekly Arctic sea-ice thickness data record from merged CryoSat-2 and SMOS satellite data. *The Cryosphere*, *11*(4), 1607–1623. https://doi.org/10.5194/tc-11-1607-2017

Schodlok, M. P., Hellmer, H. H., Rohardt, G., & Fahrbach, E. (2006). Weddell Sea iceberg drift: Five years of observations. *Journal of Geophysical Research*, *111*(C6). https://doi.org/10.1029/2004JC002661

Smith, G. C., Roy, F., Mann, P., Dupont, F., Brasnett, B., Lemieux, J.-F., et al. (2014). A new atmospheric dataset for forcing ice-ocean models: Evaluation of reforecasts using the Canadian global deterministic prediction system: CGRF Dataset for Forcing Ice-Ocean Models. *Quarterly Journal of the Royal Meteorological Society*, *140*(680), 881–894. https://doi.org/10.1002/qj.2194

Smith, S. D. (1993). Hindcasting iceberg drift using current profiles and winds. *Cold Regions Science and Technology*, *22*(1), 33–45. https://doi.org/10.1016/0165-232X(93)90044-9

Smith, S. D., & Banke, E. G. (1983). The influence of winds, currents and towing forces on the drift of icebergs. *Cold Regions Science and Technology*, *6*(3), 241–255. https://doi.org/10.1016/0165-232X(83)90045-9

Spreen, G., Kaleschke, L., & Heygster, G. (2008). Sea ice remote sensing using AMSR-E 89-GHz channels. *Journal of Geophysical Research*, *113*(C2), C02S03. https://doi.org/10.1029/2005JC003384

Stadnyk, T. A., Tefs, A., Broesky, M., Déry, S. J., Myers, P. G., Ridenour, N. A., et al. (2021). Changing freshwater contributions to the Arctic: A 90-year trend analysis (1981–2070). *Elementa: Science of the Anthropocene*, *9*(1), 00098. https://doi.org/10.1525/elementa.2020.00098

Stern, A. A., Adcroft, A., & Sergienko, O. (2016). The effects of Antarctic iceberg calving-size distribution in a global climate model. *Journal of Geophysical Research: Oceans*, *121*(8), 5773–5788. https://doi.org/10.1002/2016JC011835

Tang, C. C., Ross, C. K., Yao, T., Petrie, B., DeTracey, B. M., & Dunlap, E. (2004). The circulation, water masses and sea-ice of Baffin Bay. *Progress in Oceanography*, *63*(4), 183–228. https://doi.org/10.1016/j.pocean.2004.09.005

The NEMO Team. (2024). NEMO version 4.2.2. [Software]. https://forge.nemo-ocean.eu/nemo/nemo/-/releases/4.2.2

Tschudi, M., & Univ Of CO. (2019). *Polar pathfinder daily 25 km EASE-grid Sea Ice motion vectors*. NASA National Snow and Ice Data Center Distributed Active Archive Center. https://doi.org/10.5067/INAWUWO7QH7B

Turnbull, I. D., Fournier, N., Stolwijk, M., Fosnaes, T., & McGonigal, D. (2015). Operational iceberg drift forecasting in Northwest Greenland. *Cold Regions Science and Technology*, *110*, 1–18. https://doi.org/10.1016/j.coldregions.2014.10.006

Vinje, T. E. (1980). Some satellite-tracked iceberg drifts in the Antarctic. *Annals of Glaciology*, *1*, 83–87. https://doi.org/10.3189/S026030550001702X

Wagner, T. J. W., Dell, R. W., & Eisenman, I. (2017). An analytical model of iceberg drift. *Journal of Physical Oceanography*, *47*(7), 1605–1616. https://doi.org/10.1175/JPO-D-16-0262.1

Wagner, T. J. W., Wadhams, P., Bates, R., Elosegui, P., Stern, A., Vella, D., et al. (2014). The "footloose" mechanism: Iceberg decay from hydrostatic stresses. *Geophysical Research Letters*, *41*(15), 5522–5529. https://doi.org/10.1002/2014GL060832

Wesche, C., & Dierking, W. (2016). Estimating iceberg paths using a wind-driven drift model. *Cold Regions Science and Technology*, *125*, 31–39. https://doi.org/10.1016/j.coldregions.2016.01.008

Yankovsky, A. E., & Yashayaev, I. (2014). Surface buoyant plumes from melting icebergs in the Labrador Sea. *Deep Sea Research Part I: Oceanographic Research Papers*, *91*, 1–9. https://doi.org/10.1016/j.dsr.2014.05.014

Yulmetov, R., Marchenko, A., & Løset, S. (2016). Iceberg and sea ice drift tracking and analysis off north-east Greenland. *Ocean Engineering*, *123*, 223–237. https://doi.org/10.1016/j.oceaneng.2016.07.012

Zeinali Torbati, R., Turnbull, I. D., Taylor, R. S., & Mueller, D. (2020). Evaluation of the relative contribution of meteorological and oceanic forces to the drift of ice islands offshore Newfoundland. *Journal of Glaciology*, *66*(256), 203–218. https://doi.org/10.1017/jog.2019.96